Simulation of Nonisothermal Flow of Melt During Melting Process of Vibration-Induced Polymer Extruder

Yan-hong Feng, Jin-ping Qu, He-zhi He, Gang Jin, Xian-wu Cao, Jian Song

National Engineering Research Center of Novel Equipment for Polymer Processing, The Key Laboratory of Polymer Processing Engineering of Ministry of Education, South China University of Technology, Guangzhou, China

Received 15 March 2006; accepted 5 April 2006
DOI 10.1002/app.24891
Published online in Wiley InterScience (www.interscience.wiley.com).

ABSTRACT: A simplified 2D melt film model was established to simulate the nonisothermal melt flow during the melting process of the vibration-induced polymer extruder of which the screw can vibrate axially. Since polymer has time-dependent nonlinear viscoelastic characteristic with vibration force filed (VFF), a self-amended nonisothermal Maxwell constitutive equation that can reflect the relaxation time spectrum of polymer was adopted. Using the 2D melt film model, melt films of two kinds of thickness representing different melting stages were simulated to investigate the influence tendency of the same VFF on the different melting stage. Special flow patterns and temperature distribution of melt in the melt film between the driving wall and the solid/melt interface with various vibration force fields were systematically simulated. It is found out that within a certain range of vibration strength, the application of vibration can optimize the time-averaged shear-rate distribution, improve the utilization efficiency of energy, and promote melting process; and the thinner the melt film is, the more intense the nonlinear viscoelastic response becomes with the same VFF; moreover, there exists optimum vibration strength to make the melting process fastest, which is in accord with the visualization experimental results. © 2006 Wiley Periodicals, Inc. J Appl Polym Sci 102: 5825–5840, 2006

Key words: vibration force field; extrusion; dynamic melting; finite element method; viscoelasticity; amended nonisothermal Maxwell constitutive equation

INTRODUCTION

The application of vibration technology to the polymer processing so as to improve the processing behavior of the polymer has been attracting more and more attention recently. The most direct vibration technology is to impose parallel or orthogonal sound or ultrasonic oscillation in the extrusion dies.[1–4] Ibar[5] reviewed the melt vibration technology at low frequency. The researches on the practical applications of melt vibration technology on the extrusion process proved that the effect of oscillations can reduce the viscosity of melt, diminish die swell, lower die pressure, and enhance the mechanical properties of extrudate. Li and coworkers[6,7] found out that the appearance of PS, HDPE, and LLDPE extrudates are greatly improved in presence of ultrasonic waves. The ultrasonic oscillations can greatly improve the processabilities of PS, HDPE, LLDPE, and PS/HDPE blends, and enhance the compatibility and mechanical properties of PS/HDPE blends.

Correspondence to: Y.-H. Feng (yhfeng@scut.edu.cn).

Contract grant sponsor: Guangdong Nature Science Foundation; contract grant number: 04300096.

Contract grant sponsor: National Natural Science Foundation of China; contract grant number: 10472034.

© 2006 Wiley Periodicals, Inc.

The above researches are mainly on the effects of melt vibration technology applied in polymer processing. On the other hand, the oscillatory shear flow is also widely used to exam various non-Newtonian model, aiming at accurately describing the nonlinear viscoelastic characteristic of polymer. Rahaman and Ramkissoon[8] used upper-convected Maxwell fluid as non-Newtonian model to investigate the flow of a fluid in pipes of uniform circular cross section when the pressure gradient is pulsating, and found out that the velocity distribution for the upper-convected Maxwell fluid is not in phase with the exciting pressure distribution. Subbotin et al.[9] used a Rouse-like model of chains with finite extensibility to study the nonlinear dynamics of confined polymer melts under oscillatory flow and calculated elastic and dissipative stresses and corresponding storage and loss moduli. Orbey and Dealy[10] compared three procedures for determining a set of relaxation times and discrete moduli from a small-amplitude oscillatory shear experiment to determine the parameters of a generalized Maxwell model. And it was found out that the nonlinear regression can give a good fit of the data with a minimum number of parameters. Wong and Isayev[11] studied the orthogonal superposition of small and large amplitude oscillations upon steady shear flow of elastic fluids, and obtained the theoretical results using the Leonov viscoelastic constitutive equation.

For a polymer melt in oscillatory shear at small strain amplitudes, the stress response is linear and sinusoidal, and this is called small-amplitude oscillatory shear (SAOS). At higher strain amplitudes, the shear stress wave is nonlinear and nonsinusoidal, and this is called large amplitude oscillatory shear (LAOS).[12] As a useful tool for the study of nonlinear viscoelasticity in polymeric liquids, LAOS has excited more and more interest. Giacomin and coworkers[13–19] described nonlinear rheologic behavior in LAOS of several polymer melt using transient network structural theory and upper convected Maxwell constitutive equation. Atalık and Kuenings[20] performed a nonlinear study of planar LAOS flow using the Giesekus and Johnson-Segalman models, and pointed out that the wall slip is not a necessary condition for the occurrence of even harmonics.

In a vibration-induced polymer extruder (VIPE),[21–23] a vibration exciter is connected with its screw, and a sinusoidal velocity in axial direction is superposed on the steady rotation of screw; thus the screw rotates pulsantly with variable frequency and amplitude that can be changed conveniently according to the rheologic property of the polymer, and the vibration force field is applied to the entire extrusion process, as shown in Figure 1. This kind of oscillation of screw is different from that of the Buss reciprocating extruder of which the vibration frequency depends on the rotation speed of its screw. In single-screw extruders, the melting zone of the screw plays an important role for both product quality and processing benefits. We call the melting process in the VIPE ''the dynamic melting process'' (DMP) and the conventional melting without VFF ''the steady melting process'' (SMP). Although the conventional melting theory has had a full development,[24–31] it cannot be used to describe the special melting process in VIPE accurately for the following two reasons:

- The melting process is considered to be stable in the conventional researches of melting mechanism, and nonisothermal pure viscous constitutive equations are mostly used. During the DMP, the screw rotates pulsatively, which causes the velocity field in melt change periodically, and further causes the apparent viscosity and relaxation time change periodically, so the flowing behavior during the DMP is time-dependent viscoelastic; thus, the hypothesis of pure viscous property of melt will not be suitable any more.
- The DMP is periodic, and the transient effect should be considered.

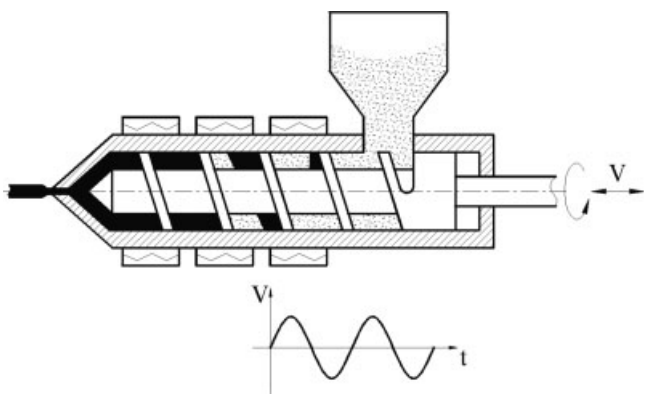

Figure 1 Diagrammatic sketch of VIPE.

Therefore, the DMP is a nonlinear, nonisothermal, close coupled transient problem. In our previous work, a simplified 2D melting model was established, and the DMPs with several vibration parameter combinations were simulated.[32] The simulation results reveal that for the vibration parameter combinations simulated the application of the VFF to extrusion process can optimize the distribution of shear rate in the flow field by reducing the shear rate near the driving wall surface and enhancing the shear rate near the solid/melt interface, which is in favor of the dynamic removal of the newly-generated melt at the solid/melt interface and also generates a great deal of heat, thus accelerating melting process. On the other hand, when the authors tried to further increase the frequency and amplitude of the simulation with the 2D dynamic melting model, it became difficult to achieve convergence; however, it was noticed that the effect of VFF on the melting process is mainly brought out by the special melt conveying behavior and the consequent variation of temperature field, which is a result of nonlinear viscoelastic response of melt to VFF, and it is considered that the influence of VFF on solid conveying is relatively small, since the resistibility of solid phase will be much higher than that of melt. Thus, in this work, a local melt film model was put forward from the dynamic melting model to reflect the variation characteristic of the melt conveying and temperature distribution of the melt film between the driving wall and the solid/melt interface, so as to reveal the active mechanism of VFF on the melting process. In addition, visualization experiments were carried out, and the theoretical results were compared with the experimental results.

MATHEMATICAL MODEL

The 2D melt film mode is illustrated in the Figure 2. The x direction is the conveying direction of the melt in the melt film; y direction is the depth direction of the melt film. The upper boundary represents the driving surface moving pulsantly in the positive

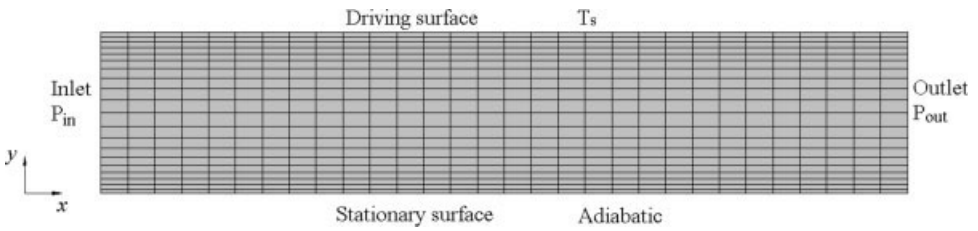

Figure 2 2D melt film model.

direction of the x coordinate. The lower boundary is relative stationary.

To build up the mathematical model the following assumptions were made:

- The influence of the gravity can be neglected.
- The melt is incompressible, and the density of the melt keeps constant.
- There is no slip at the wall.

According to these assumptions, the flow field of the melt in the melt film can be described as

$$\frac{\partial \rho}{\partial t} + \frac{\partial}{\partial x}(\rho v_x) + \frac{\partial}{\partial y}(\rho v_y) = 0 \tag{1}$$

The equations of motion are

$$\rho\left(\frac{\partial v_x}{\partial t} + v_x\frac{\partial v_x}{\partial x} + v_y\frac{\partial v_x}{\partial y}\right) = -\frac{\partial p}{\partial x} + \left(\frac{\partial \tau_{xx}}{\partial x} + \frac{\partial \tau_{xy}}{\partial y}\right) \tag{2}$$

$$\rho\left(\frac{\partial v_y}{\partial t} + v_x\frac{\partial v_y}{\partial x} + v_y\frac{\partial v_y}{\partial y}\right) = -\frac{\partial p}{\partial y} + \left(\frac{\partial \tau_{xy}}{\partial x} + \frac{\partial \tau_{yy}}{\partial y}\right) \tag{3}$$

The equation of energy is

$$\rho C_p \frac{DT}{Dt} = \frac{Dp}{Dt} + \nabla(k\nabla T) + (\boldsymbol{\tau} : \nabla \mathbf{v}) \tag{4}$$

where ρ, C_p, and k are the mass density, specific heat, and thermal conductivity of melt, respectively; v_x and v_y are the velocity components in the x and y directions, respectively; t is the time; p represents the pressure; T is the temperature; $\boldsymbol{\tau}$ represents stress tensor.

Boundary conditions

Boundary conditions of velocity

The upper boundary is the driving surface moving pulsantly in the positive direction of the x coordinate. According to the no-slip assumption, the velocity boundary conditions can be given as

$$v_x\big|_{y=\delta} = v_x^0 + v_{xA}^*\Big|_{y=0} \tag{5}$$

$$v_y\big|_{y=\delta} = 0 \tag{6}$$

$$v_{xA}^*\big|_{y=\delta} = a\ 2\pi f\ \sin(2\pi f t) \tag{7}$$

where v_x^0 is the average velocity in the x-direction that can also be called the balance velocity (namely, the velocity of steady state), $v_x|_{y=\delta}$ and $v_y|_{y=\delta}$ are the velocity components at the driving surface in the x and y-directions, respectively. $v_{xA}^*|_{y=\delta}$ is the vibration velocity of the driving surface in the x-direction, δ is the thickness of the melt film, f is the vibration frequency, and a is the vibration amplitude.

The lower boundary is relatively stationary. The boundary conditions of velocity at this boundary can be given as

$$v_x\big|_{y=0} = v_y\big|_{y=0} = 0 \tag{8}$$

where, the $v_x|_{y=0}$ and $v_y|_{y=0}$ are the velocity components at the lower boundary in the x and y-directions, respectively.

Thermal boundary conditions

1. Apply constant temperature T_s at the driving surface.
2. At the very beginning, the stationary boundary was used to represent the solid/melt interface, and the temperature of this boundary was set as the melting point. The simulation results revealed that because the melt film is very thin, the temperature field of the melt film was primarily dominated by this stationary boundary of lower temperature, and most of the heat of dissipation transferred out from this boundary, namely the effect of heat conduction concealed that of the dissipation heat generated by the application of VFF; therefore, the temperature difference between the dynamic melt conveying

and steady melt conveying became too small to compare; in fact, in the melting model, this part of heat should be used to heat the solid material, but in the melt film model, there is no way to calculate this part of heat. Therefore, in the melt film model, the thermal boundary at the stationary boundary is set adiabatic, namely, no heat gets in or out from this interface, which can reflect the heat of viscous dissipation, especially the heat of dynamic dissipation, moreover, this kind of thermal boundary condition has little influence on the study of the characteristic of the velocity distributions in the melt film with VFF.

Pressure boundary conditions

Because the pressure fluctuation in the extrusion direction caused by VFF is almost in-phase, that is, the absolute pressure values of two points within a pretty short distance in the extrusion direction will vary in synchronism, and the corresponding relative pressure difference changes very little; therefore, the transient pressure gradient can be assumed to be constant. Thus, the pressure difference between the inlet and outlet is used as pressure boundary condition, and higher pressure p_{out} is applied to the outlet that is close to the extruder head; lower pressure p_{in} is applied to the inlet that is close to the feed section.

Constitutive equations

While simulating the melt flow during DMP, constitutive equation that can reflect the time-dependent viscoelastic characteristic must be used. Formally, the White-Metzner constitutive equation is quite like the upper-convected Maxwell model, but in fact the White-Metzner constitutive equation treats the relaxation time and viscosity as functions of shear rate; thus, this betterment can reflect the experimental result of multirelaxation-spectrum. Referring to the White-Metzner constitutive equation, the linear-viscoelastic Maxwell constitutive equation[33] was amended as

$$\boldsymbol{\tau} + \lambda(\dot{\gamma}, T)\frac{\partial \boldsymbol{\tau}}{\partial t} = 2\eta(\dot{\gamma}, T)\boldsymbol{d} \tag{9}$$

where $\lambda(\dot{\gamma}, T) = \eta(\dot{\gamma}, T)/G$ is the relaxation time, G is the bulk modulus, $\boldsymbol{d} = (\boldsymbol{L} + \boldsymbol{L}^T)/2$ is the strain rate tensor with $\boldsymbol{L} = (\bigtriangledown \boldsymbol{v})^T$, $\dot{\gamma} = \sqrt{2\boldsymbol{d}:\boldsymbol{d}^T}$ is the shear rate, which is the second invariant of strain rate tensor $\boldsymbol{d}$. $\eta(\dot{\gamma}, T)$ is the apparent viscosity, which is a function of shear rate and temperature. Taking the influence of temperature on viscosity into consideration, the Cross-Arrhenius empirical formula[34] was used to describe the variation of melt viscosity from η_0 to η_∞, thus, obtains the $\eta(\dot{\gamma}, T)$ in eq. (9) as

$$\eta(\dot{\gamma}, T) = \alpha_T\left(\eta_\infty + \frac{\eta_0 - \eta_\infty}{1 + c\dot{\gamma}^m}\right) \tag{10}$$

where, α_T is the transfer factor of temperature, η_0 and η_∞ are the zero-shear-rate viscosity and second Newtonian viscosity, c and m are characteristic constants of the material. Usually η_∞ cannot be obtained by experiment, and used to be set as an arbitrary constant.

$$\alpha_T = \exp[b(T_r - T)] \tag{11}$$

where b is the sensitive coefficient of temperature, T_r is the reference temperature, which is set as melting point T_m. To obtain the parameters in the Cross-Arrhenius model, rheologic experiments at different temperatures should be taken. Through the rheologic experiments, the different apparent viscosities corresponding to different shear rates at different temperatures can be obtained. The second Newtonian viscosity can be set as a constant. Then, the parameters of the Cross-Arrhenius model can be finally obtained by nonlinear fitting. Thus, the apparent viscosity can be described as

$$\eta(\dot{\gamma}, T) = \exp[b(T_m - T)]\left(\eta_\infty + \frac{\eta_{T_m 0} - \eta_\infty}{1 + c\dot{\gamma}^m}\right) \quad T \geq T_m \tag{12}$$

Since the stress can not be described as the explicit function of velocity and gradient of velocity when simulating the viscoelastic flow, the stress is a variable to be solved, which causes the nonlinear characteristics of viscoelastic flows and calls for more challenge and more computer resources than those numerical simulation of Newtonian flows and generalized Newtonian flows. According to weather the stress is an original variable, the finite element methods for the viscoelastic flows can be divided into mixed method and split method.

In this work, the split method[35–39] is adopted; the velocity and pressure are the two variables to be solved. Thus the Galerkin weak form of the above problem can be stated as: to obtain the $(n + 1)$th iterative value $(\boldsymbol{v}^{(n+1)}, p^{(n+1)}) \in V \times P$, the following equations must be satisfied,

$$\int_\Omega (2\eta_{\text{ref}}\boldsymbol{d}^{(n+1)} : \nabla\phi_u - p^{(n+1)}\nabla\phi_u)\, d\Omega = \int_{\partial\Omega} \boldsymbol{F}\phi_u d\, \partial\Omega + \int_\Omega \boldsymbol{f}\phi_u\, d\Omega - \int_\Omega \boldsymbol{\tau}^* : \nabla\phi_u\, d\Omega, \quad \forall\phi_u \in V \tag{13}$$

$$\int_\Omega (\nabla \boldsymbol{v}^{(n+1)})\varphi_p\, d\Omega = 0, \quad \forall\varphi_p \in P \tag{14}$$

TABLE I
Screw Geometries

Diameter D (mm)	Pitch angle θ	Feed section depth H_1 (mm)	Metering section depth H_3 (mm)	Melting section length L (mm)	Channel width W (mm)	Flight width e (mm)
20	17.65°	3.2	1.1	120	17	2

where ϕ_u and ϕ_p are the shape functions of velocity and pressure, respectively, V and P are the function spaces of $\mathbf{v}$, p defined in domain Ω, η_{ref} is the reference viscosity, namely $\eta(\dot{\gamma}, T), \boldsymbol{\tau}^* = \boldsymbol{\tau} - 2\eta_{ref}\boldsymbol{d}^n$, the extra stress $\boldsymbol{\tau}$ can be solved using the constitutive eq. (9) with the former iterative value ($\mathbf{v}^n$, p^n).

This constitutive equation program not only takes the viscoelastic characteristic of polymer into account, but also reflects the relaxation spectrum.

Meshing

By extracting local melt film model from dynamic melting model, the research can be further focused on the melt of which the nonlinear viscoelastic behavior is more obvious with VFF, which gives prominence to the key points. The meshes of the established local melt film model can be further refined to capture more delicate viscoelastic behavior. As shown in Figure 2, the local refinement near the upper and lower boundaries can help to capture the nonlinear viscoelastic flow of the melt. The whole model was divided into 600 elements.

EXPERIMENT AND EXPERIMENTAL RESULTS

To investigate the effect of VFF on the melting process, visualization experiments were carried out on a VIPE of which the barrel can be half-opened. Table I lists out the geometrical configuration of the compression section of the screw used in the experiments. For the study, two pressure transducers were mounted on the wall of the barrel corresponding to the start point and end point of compression section of screw. The low-density polyethylene (LDPE) banded 951-050 was used. The physical properties of the LDPE melt are listed in the Table II.

The procedure of the visualization experiment is given below:

i. Mix a small percentage of carbon black with LDPE.
ii. Set the rotate speed of screw 60 rpm. Set the temperatures of the compression section, metering section and die 140, 180, and 170°C, respectively.
iii. Switch on the vibration exciter, and set the vibration frequency and amplitude. Omit this step for the conventional extrusion without VFF.
iv. Extrude until steady state is reached.
v. Store the transient pressures at the start point and the end point of the compression section of screw.
vi. Stop screw rotation and cool the barrel quickly.
vii. Open the upper half of the barrel. Peel the exposed material belts in the upper half screw pitches of the melting section away.
viii. Slice the material belts perpendicular to the flights.
ix. Measure the area of the unmelted plastic and divide it by the channel cross section area, then obtain the melting profile.

It should be pointed out that our main purpose of this work is to found out the effects of vibration parameters on the melting process; thus, we only chose one kind of rotate speed as well as the temperature settings in the experiments, and changed the vibration frequency and amplitude, so that there should be no other factors to affect the melting process except the vibration frequency and amplitude.

In Figure 3, the melting profiles of DMP obtained form the visualization experiment are compared with the melting profile of SMP, which shows that the application of VFF to the melting process can reduce the melting length. The effects of the vibration parameters on the melting process are given in Figure 4 by the comparison of the decrement rates of the melting length caused by various vibration parameters. For the case when frequency is 5 Hz, the decrement rate of melting length increases almost proportionally with the increase in amplitude from 0.05 to 0.15 mm; however, with the further increase in amplitude, the variation of the decrement rate becomes irregular. For the case when frequency is 10 Hz, the similar variation pattern is found as above. Irregular variation of decrement rate is found for the case of higher frequency 20 Hz, while amplitude increases from 0.05 to 0.2 mm. On the other hand, for the case when the amplitude is 0.05 mm, the decrement rate increases with the increase in

TABLE II
Physical Properties of LDPE (951-050) Melt

Density ρ (kg/m^3)	Melting point T_m (°C)	Thermal conductivity k (W/m °C)	Specific heat C_p (kJ/kg °C)
810	110	0.24	2.43

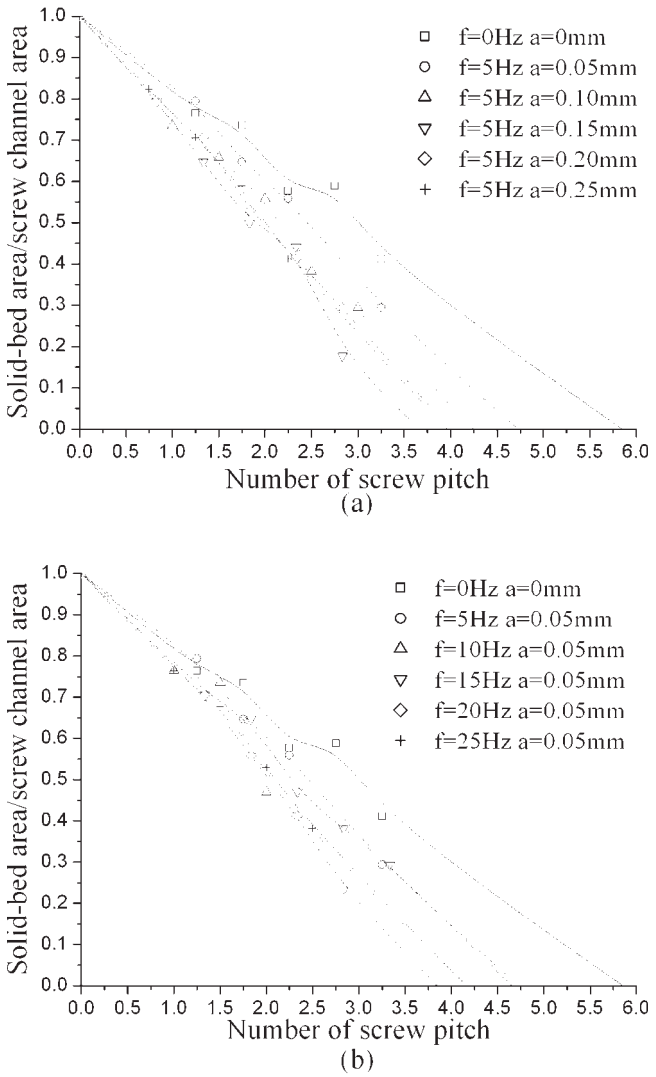

Figure 3 Experimental melting profiles.

vibration frequency from 5 to 20 Hz; when the amplitudes are 0.1 and 0.15 mm, the decrement rate increases with the increase in the vibration frequency from 5 to 10 Hz; however, the further increase in frequency from 10 to 20 Hz results in a decrease in decrement rate; for the cases of larger amplitudes, namely, 0.2 and 0.25 mm, the variations of decrement rate are irregular when the frequency increases from 5 to 20 Hz. In this article, we define the product of vibration frequency and amplitude as vibration strength that presents the variation amplitude of pulsant velocity. The above experimental data indicate that when the vibration strength is comparatively small, the increases in frequency and amplitude can further accelerate the melting process and shorten the melting length; however, when the vibration strength exceeds certain value, the decrement of melting length becomes irregular with the further increase in frequency and amplitude. There exists optimum vibration strength to make the melting process fastest. This phenomenon is considered to be related to the nonlinear viscoelasticity of the polymer.

SAMPLE RESULTS OF SIMULATION AND DISCUSSION

In this section, illustrative results obtained from the simulation approach described above are provided. For the calculations, the LDPE banded 951-050 was chosen for simulation. The physical properties of the LDPE melt are listed in the Table II. Rheologic experiments at different temperatures were taken. The second Newtonian viscosity was set $\eta_\infty = 20$ Pa s. Then the Cross-Arrhenius model was finally obtained by nonlinear fitting

$$\eta(\dot{\gamma}, T) = \exp[0.0117(110 - T)]\left(20 + \frac{50530 - 20}{1 + 1.6677\dot{\gamma}^{0.6758}}\right) \tag{15}$$

The vibration parameters for simulation were chosen as two groups: (1) Keep the frequency as 25 Hz, and set the amplitudes as 0.05, 0.1, 0.15, 0.2, and 0.25 mm, respectively. (2) Keep the amplitude as 0.25 mm, and set the frequencies as 5, 10, 15, 20, and 25 Hz, respectively. Thus, the influence of amplitude changes on the melting process with the fixed frequency and the influence of frequency changes on the melting process with the fixed amplitude can be compared.

Geometry parameters and boundary conditions

The 2D melt film model presented in this work is aimed to qualitatively reveal the active mechanism of VFF on the melting process. During the melting process, the thicknesses of the melt film and melt

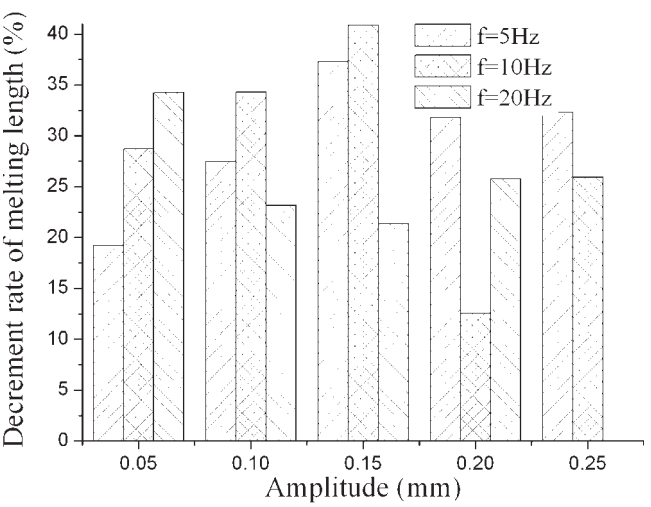

Figure 4 Ratios of the decrements of melting length of various DMPs to the melting length of SMP.

pool keep changing, which causes the apparent viscosity of melt also keep changing. Because the polymer melt is of viscoelastic, its relaxation time is in connection with viscosity, and thus the relaxation time during different melting stages and at different melt regions are different, causing the response of melt to the same VFF change correspondingly. In this article, two melt films of typical thickness were chosen to carry out the 2D nonisothermal melt flow analyses with several typical vibration force fields. To simulate the velocity and temperature distributions of the melt film when the rotate speed of screw is 60 rpm, the geometry parameters of the melt film and boundary conditions should be determined according to the actual experimental conditions.

Thin melt film representing the initial stage of melting process

Set the thickness of melt film in Figure 2 $\delta = 0.2$ mm, indicating the upper melt film adjacent to the barrel during the initial stage of the melting process, and the length of the model is 1 mm. The upper boundary moves in the positive direction of x coordinate, and the steady speed without vibration $v_x^0 = 0.06$ m/s. The lower boundary was set to be stationary. The temperature of the moving boundary was set as 140°C. The stationary boundary was assumed to be adiabatic to fully reflect the effect of temperature increment caused by the VFF. The pressure difference between the inlet and outlet was taken as 0.025 MPa, which was set according to the length of the thin melt film model and the average pressure gradient measured from the experiments when the rotate speed of screw was 60 rpm.

Thick melt film representing the late stage of melting process

Set the thickness of melt film in Figure 2 $\delta = 1$ mm, indicating the melt film adjacent to the barrel during the late stage of the melting process, and the length of the model is 5 mm. The velocity and thermal conditions were the same as that of the thin melt film model. The pressure difference between the inlet and outlet was taken as 0.125 MPa, which was also set according to the length of the thick melt film model and the average pressure gradient measured from the experiments when the rotate speed of screw was 60 rpm.

Simulation results

Velocity field results

Figure 5 shows the velocity along the depth of melt film varying within a vibration period with different vibration parameters. Figure 6 shows the velocity profiles along the melt film at different time with different vibration parameters. Figure 5(a–d) and Figure 6(a–d) are velocity results of thin melt film, Figure 5(e–f) and Figure 6(e–f) are velocity results of thick melt film. Figures 5(d) and 6(d) are the velocity simulation results using Cross-Arrhenius constitutive equation with vibration frequency being 25 Hz and amplitude being 0.25 mm. As shown in the Figure 5, the curves changing periodically represent transient velocities at certain positions along the depth of melt film; those straight lines corresponding to the curves represent the average velocities at those positions. Those topmost curves represent the pulsant velocities applied by the driving surface. In Figure 5(d), the changes of velocities of the inner melt are in-phase with the change of velocity at the driving surface, while in the Figure 5(a–c), compared with Figure 5(d) for the same position, the changes of velocities of the inner melt lags behind the change of velocity at the driving surface. As seen from Figure 6(a–c), because of the viscoelastic characteristic of polymer, the velocity profiles during the velocity increasing stage will not superpose on the velocity profiles during the velocity decreasing stage, even though the driving velocities are the same at these time points. And even at the time points when the transient driving velocities equal the steady driving velocity, the transient velocity distribution profiles for the velocity increasing stage and velocity decreasing stage don't superpose on the velocity profile of steady state. This phenomenon can be explained as follows. During the steady extrusion process, the velocity distribution is fully developed, which will not change with time, whereas when the VFF is applied, the velocity applied at the boundary will change with time. As we all know, the melt flows by means of the movements of the chain segments of macromolecules that change the conformations of the macromolecular chains and cause the movements of the centers of gravity of macromolecular chains, this kind of movement has relaxation characteristic, and it must spend a certain period of time for the motion of macromolecule to reach balance which is quite different from the motion mode of micromolecule which can reach the balance position instantly. Taking the starting stage of shear flow for example, it also will take some time for the velocity distribution in melt film to reach the balance velocity, namely the flow field is fully developed. It is just this characteristic causes that while being driven by the alternating velocity boundary condition the inner melt can not reach the same balance velocity as the steady extrusion even at the moment the transient velocity is the same as that of the steady extrusion, this phenomenon is called hysteresis in this article. When the vibration strength is

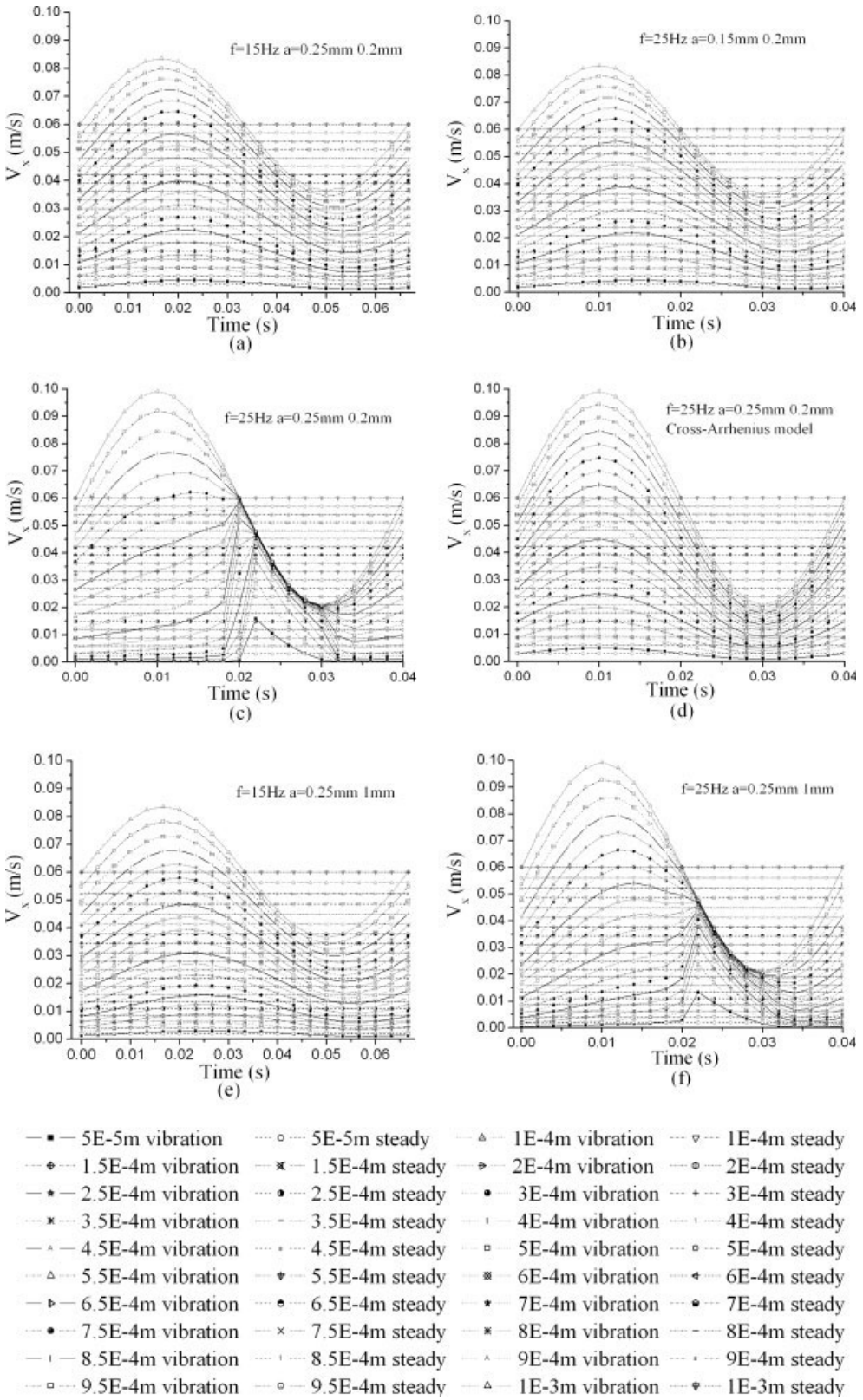

Figure 5 Velocity curves along the depth of the thin and thick melt films varying within a vibration period with different vibration parameters (a) $f = 15$ Hz, $a = 0.25$ mm, $\delta = 0.2$ mm; (b) $f = 25$ Hz, $a = 0.15$ mm, $\delta = 0.2$ mm; (c) $f = 25$ Hz, $a = 0.25$ mm, $\delta = 0.2$ mm; (d) $f = 25$ Hz, $a = 0.25$ mm, $\delta = 0.2$ mm, with Cross-Arrhenius constitutive equation; (e) $f = 15$ Hz, $a = 0.25$ mm, $\delta = 1$ mm; (f) $f = 25$ Hz, $a = 0.25$ mm, $\delta = 1$ mm.

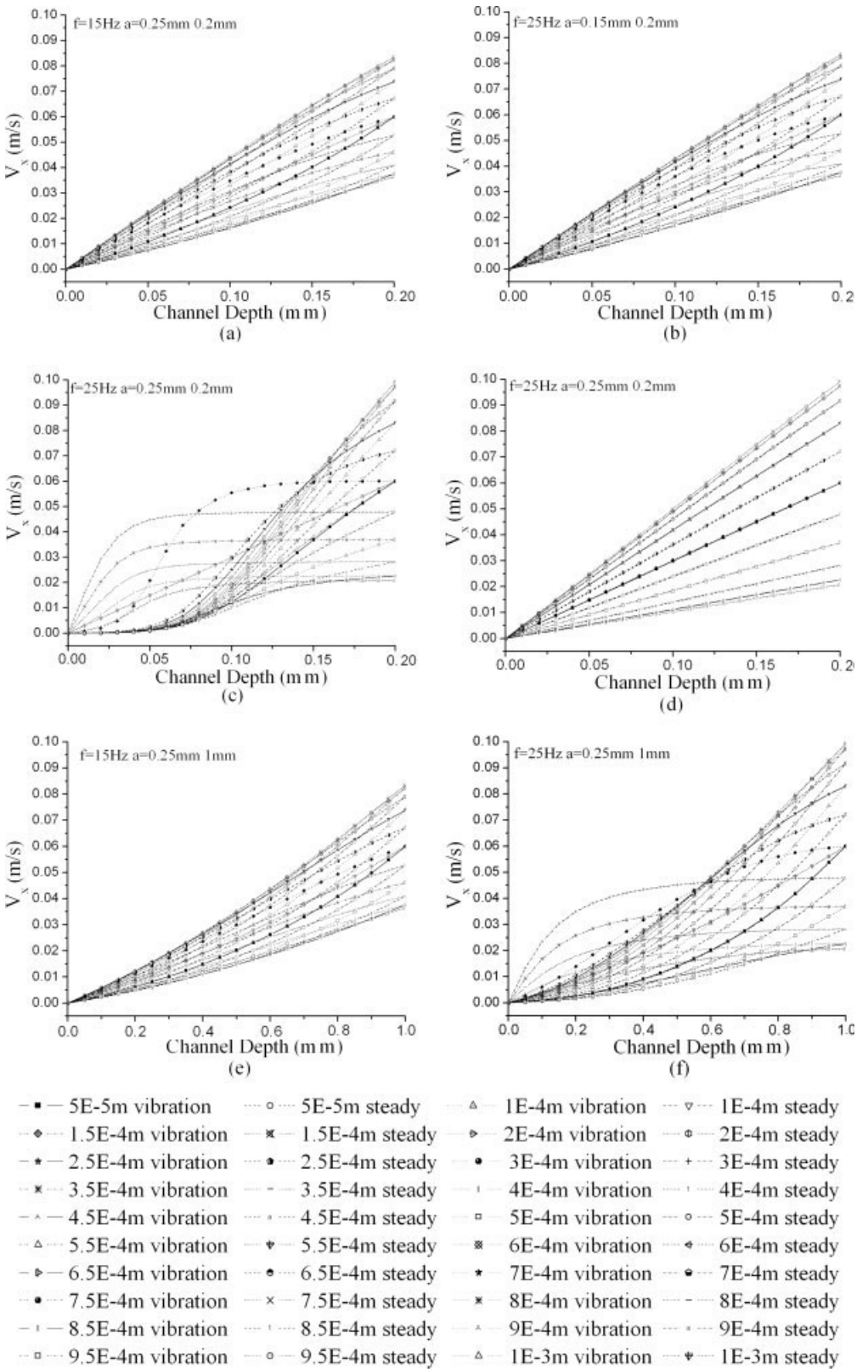

Figure 6 Velocity profiles along the depth of the thin and thick melt films at different time with different vibration parameters (a) $f = 15$ Hz, $a = 0.25$ mm, $\delta = 0.2$ mm; (b) $f = 25$ Hz, $a = 0.15$ mm, $\delta = 0.2$ mm; (c) $f = 25$ Hz, $a = 0.25$ mm, $\delta = 0.2$ mm; (d) $f = 25$ Hz, $a = 0.25$ mm, $\delta = 0.2$ mm, with Cross-Arrhenius constitutive equation; (e) $f = 15$ Hz, $a = 0.25$ mm, $\delta = 1$ mm; (f) $f = 25$ Hz, $a = 0.25$ mm, $\delta = 1$ mm.

comparatively weak, the variation of velocity of the inner melt can keep the same variation form of the velocity of the driving surface basically. But when the vibration strength increases to a certain degree, the velocity of the inner melt will change abruptly. It can also be seen that such sudden change of velocity will not happen when using the Cross-Arrhenius constitutive equations. The above comparison also indicates that the sudden change of velocity is in connection with the characteristic of relaxation of melt.

As shown in Figures 5(c) and 6(c), because the variation of the velocity of the driving boundary is too fast, the velocity of the inner melt diverges from the balance velocity far and away, and the further the melt is away from the driving surface, the more the velocity diverges from the balance velocity, causing the velocity of melt decay to zero before reaching the stationary surface, and the effect of the pulsant shear can not be further transferred into the inner melt, namely, the transmit of vibration is damped and can't reach the stationary surface. Then the melt near the stationary surface will cease flowing and form a layer of melt acting like solid, here we call this layer of melt the resting layer. However, the melt layer adjacent to the resting layer that nearer to the driving surface (called outer-resting-layer for convenience) will subject quite severe shear with the increase in the velocity of the driving surface. The macromolecules in the outer-resting-layer orient extremely and store a great deal of elastic energy. When the velocity of the driving surface begins to decrease, the former extremely stretched macromolecule chains will retract presenting elastic behavior due to the weakening of the external force, which causes the variation of the shear rate in the melt slow down, then the chain segments of macromolecules of the former resting layer adjacent to the stationary surface will have time to move, what's more, the elastic recovery of the macromolecule chains in the outer-resting-layer that have being extremely stretched also causes the velocity of the melt adjacent to the stationary surface increase suddenly. As for the macromolecules in the outer resting-layer, during the speed-down stage of the driving surface, the shear stress in the melt also decreases; thus, the extremely stretched macromolecule chains can retract, and the great deal of elastic energy stored in the macromolecules of the outer resting-layer during the speed-up stage of the driving surface will be released; the shear rate in the melt of outer resting-layer decreases rapidly, and there will form a layer of melt near the driving surface in which shear rate is relative small; then the former stretched macromolecule chains get back to coiling up state. When the driving surface speeds up again, the shear rate of the macromolecule chains near the driving surface increases again; the macromolecule chains orient gradually, and then another circle begins.

From these figures, it can be seen that when the vibration strength is relative small, the periodic variation form of the velocity field is similar as that of the simulation results in the 2D melting model,[32] but with the increase in the vibration strength, there appear sudden changes in velocity, both in the thin melt film model and in the thick melt film model. When comparing the Figure 6(a) with 6(e) and comparing the Figure 6(c) with 6(f) respectively, with the application of the same pulsant velocity boundary, the hysteresis loops formed by the velocity profiles of the thick melt film are smaller than the corresponding hysteresis loops formed by the velocity profiles of the thin melt film. The comparison of Figure 5(c) with 5(f) also shows the sudden change of velocity in the thick melt film is less severe than that in the thin melt film.

Figure 7 shows the average velocities of the thin and thick melt films during two periods with different vibration force fields. As shown in Figure 7(a), the curves changing periodically represent transient average velocities of the melt film with different vibration force fields. The straight line represents the average velocity of the melt film without VFF. It can be seen that the average velocity obtained using the Cross-Arrhenius constitutive equations is in phase with the driving velocity, and the fluctuant magnitude of the average velocity of pure viscous fluid is much larger than the fluctuant magnitude of the average velocity of viscoelastic fluid with the same VFF. When the amplitude is fixed and frequency increases, or when the frequency is fixed and amplitude increases, the magnitude of the variation of the average velocity of the melt film will increase. When the vibration strength is relatively small, the response of the velocity of the melt film will be approximately sinusoidal. When the vibration strength is quit large, the average velocity of the melt film varying with time will change abruptly; the larger the vibration strength is, the more severe the sudden change is. The comparison of Figure 7(b) with Figure 7(a) shows that the distortion of the average velocity pattern of the thick melt film from sinusoidal form is less severe than that of the thin melt film with the same VFF applied.

In the report of Atalık and Keunings,[20] it was pointed out that experimental studies of LAOS flows of polymer melts show nonlinear effects yielding multi- and quasiperiodic behavior in certain parameter ranges.[12,40] Fourier analysis of the shear stress response indicates that multiperiodicity manifests itself mainly with the presence of odd harmonics of the fundamental excitation frequency. In many cases, however, even harmonics of much smaller amplitude than the odd ones have also been observed.[40–42] Atalık and Keunings[20] investigated the combined

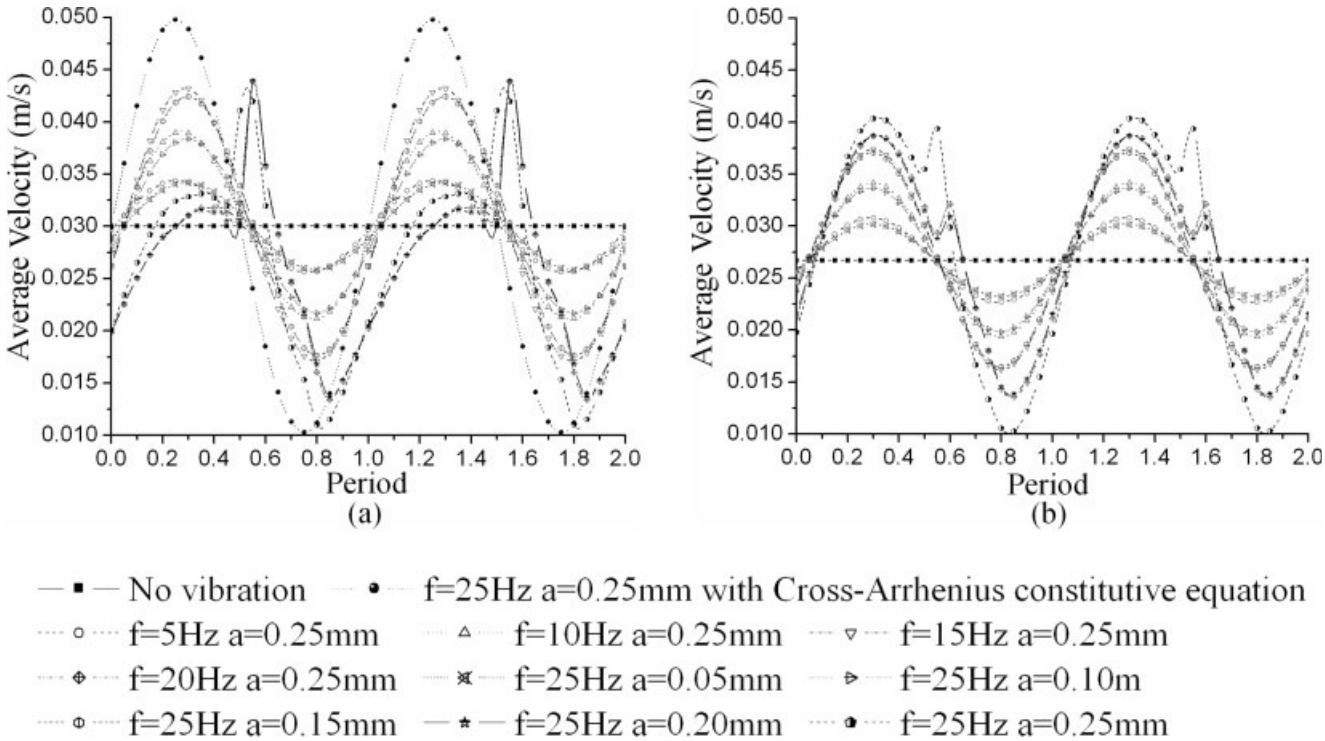

Figure 7 Average velocities of the thin and thick melt films during two periods with different vibration force fields (a) $\delta = 0.2$ mm; (b) $\delta = 1$ mm.

effects of inertia, elasticity, and shear thinning. For a very weak shear thinning and weak elasticity case, the shear stress response is nearly one periodic, and the plot of shear stress versus time is a curve quite like sine wave, as shown in Figure 8(a). Once the elasticity increases, and all other parameters being unchanged, the response of stress transits to a multiperiodic one with the appearance of the first and second odd harmonics. The plot of shear stress versus time also deformed, as shown in Figure 8(b). When the shear thinning effect is further significantly increased, the net result is an increase of the multiperiodic character of the shear stress response, as shown in Figure 8(c). For the researches on the LAOS flows, the velocity field is usually *a priori* known, namely, the shear rate is assumed to be known, and the shear stress versus shear rate loops are used to study the nonlinear response of polymer melt to LAOS flows. However, in this work, the velocity field is *a priori* unknown, and the inertial effect is taken into consideration. As we can see from the above simulation results of velocity in the melt film, the response trend of velocity to the increase in the vibration parameters is quite alike that of stress to the increase in the shear thinning and elasticity effects presented in Ref. [20]. It should be mentioned that the shear stress is symmetrical for a LAOS flow, and there are two sharp changes during a period, which occur at the positive half-period and negative half-period respectively, in Figure 8(c), because the average velocity of their driving plane is zero; however, in this work, the average velocity of the driving plane is nonzero; thus, for the cases with larger vibration parameters ($f = 20$ Hz, $a = 0.25$ mm; $f = 25$ Hz, $a = 0.2$ mm; $f = 25$ Hz, $a = 0.25$ mm), there appears only one sharp change during a period.

Results of shear rate

Figure 9 shows the time-averaged shear rate distributions along the thin melt film varying with vibration parameters. As shown in Figure 9 the degree of the influence of the VFF on the time-averaged shear rate in the melt film increases with the increase in the vibration strength. In Figure 9(a), the vibration causes the time-averaged shear rate near the driving surface decrease much more, and the time-averaged shear rate near the stationary surface decrease just a little; moreover, the time-averaged shear rate of the melt that locates in the middle of the melt film increases in a degree, and the increase in the time-averaged shear rate leans to the stationary surface. In Figure 9(b), the increase in the vibration strength causes the time-averaged shear rate near the driving surface increase, the time-averaged shear rate near the stationary surface decrease instead, and the stronger the vibration strength is, the larger the magnitude of this kind of variation of shear rate becomes. This is because the velocity in the melt film

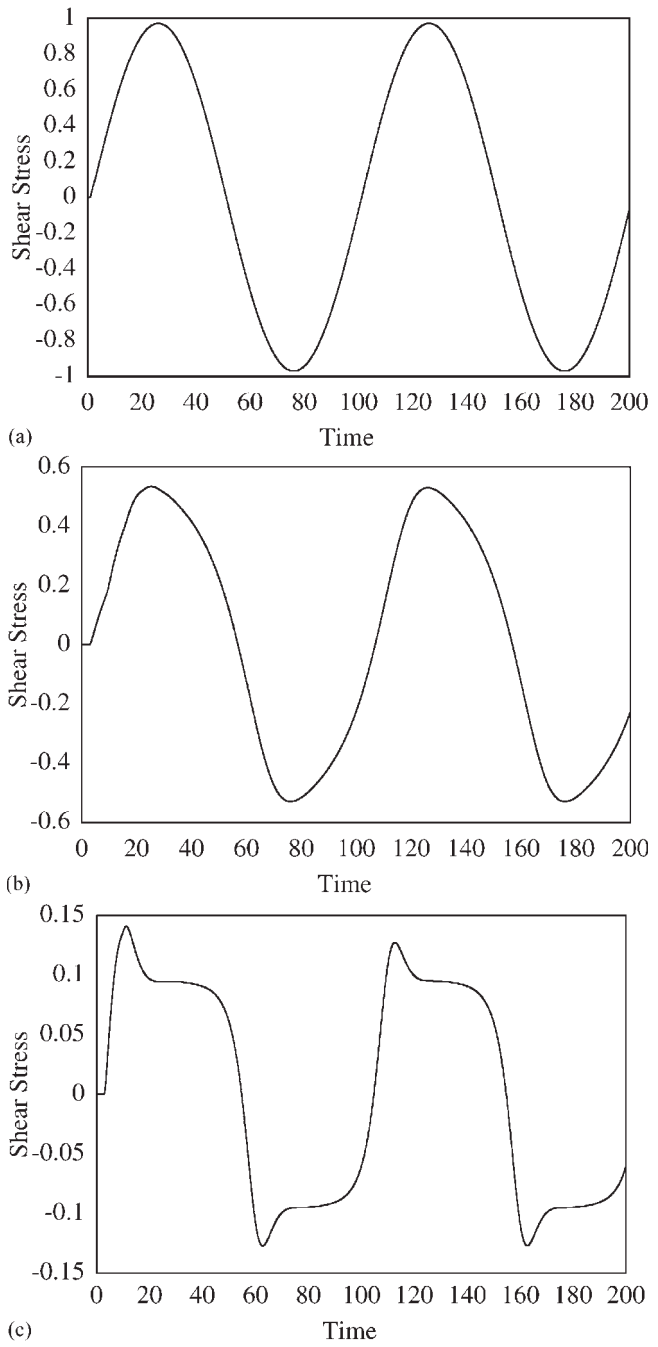

Figure 8 (a) Evolution of shear stress at fixed plate for the Giesekus model ($Re = 1$, $We = 1$, $\beta = 0.001$, $\alpha = 0.01$, $f = 0.01$) [cited from Ref. 20, Figure 1(a)]; (b) Evolution of shear stress at fixed plate for the Giesekus model ($Re = 1$, $We = 10$, $\beta = 0.001$, $\alpha = 0.01$, $f = 0.01$) [cited from Ref. 20, Figure 3(a)]; (c) Evolution of shear stress at fixed plate for the Giesekus model ($Re = 1$, $We = 10$, $\beta = 0.001$, $\alpha = 0.05$, $f = 0.01$) [cited from Ref. 20, Figure 5(a)].

will change suddenly, with the application of vibration of too strong vibration strength. As shown in Figure 9, the time-averaged shear rate in the flow field will redistribute caused by the application of VFF. Of the above five kinds of vibration parameter combinations, the amplitude 0.15 mm is the most optimum, namely, the time-averaged shear rate near the stationary surface increases, while the time-averaged shear rate near the driving surface decreases, which is in favor of the removing of the newly generated melt of lower temperature and higher viscosity and generating a great deal of heat of dynamic dissipation and thus accelerates the melting process. As for the vibration parameter combinations in Figure 9(b), on the contrary, the actions of those kinds of vibration force fields are not in favor of melting process.

The time-averaged shear rate distributions along the thick melt film varying with vibration parameters are given in Figure 10. Figure 10 shows that the variation magnitude of time-averaged shear rate in the melt film increases with the increase in vibration strength. The application of VFF causes the time-averaged shear rate of the melt adjacent to the driv-

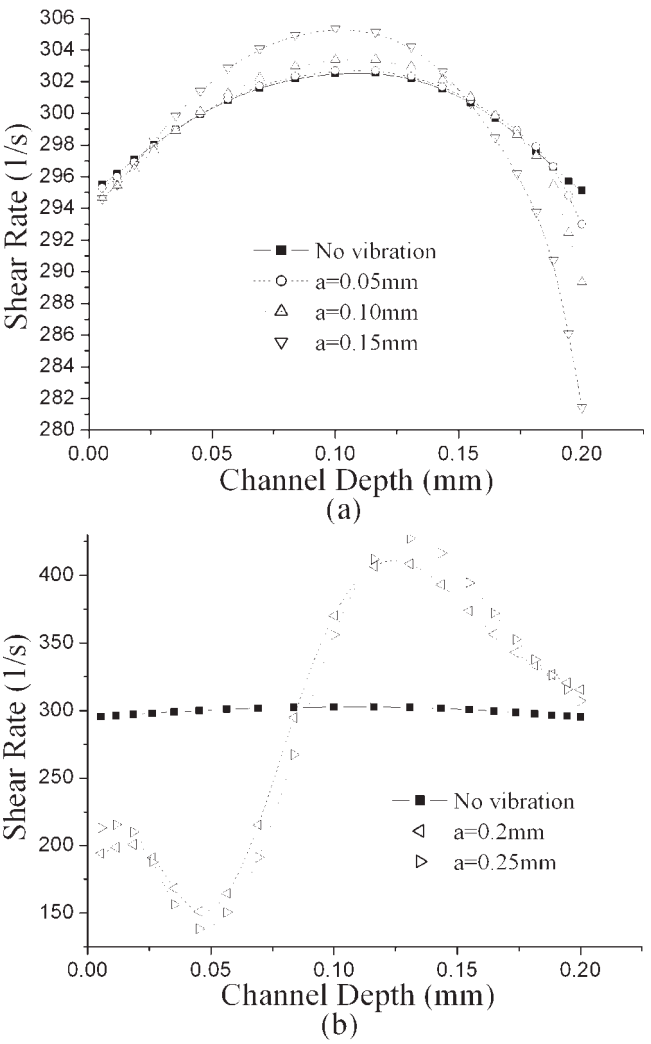

Figure 9 Time-averaged shear rate distributions along the thin melt film varying with vibration parameters, $f = 25$ Hz, $\delta = 0.2$ mm.

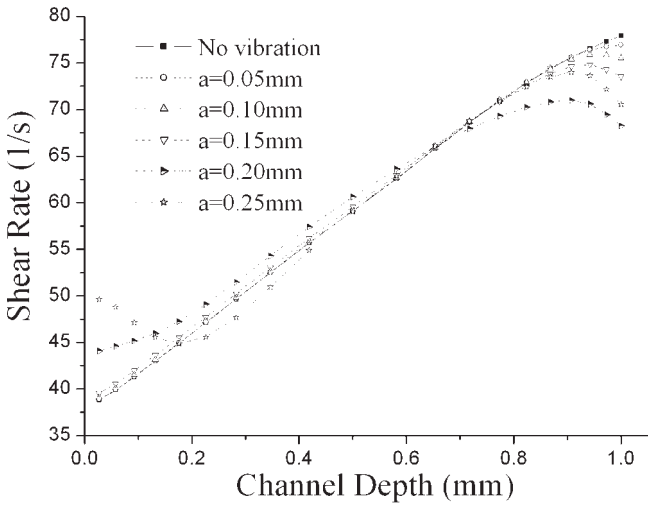

Figure 10 Time-averaged shear rate distributions along the thick melt film varying with vibration parameters, $f = 25$ Hz, $\delta = 1$ mm.

ing surface decrease, and the time-averaged shear rate of the melt adjacent to the stationary surface increase. As shown in Figure 10, when the amplitude is 0.2 mm, although there have already appeared sudden change of velocity, the VFF still cause the time-averaged shear rate of the melt adjacent to the driving surface decrease, and the time-averaged shear rate of the inner melt, especially the melt adjacent to the stationary surface, increase, and the increment is the largest among the cases calculated in the work. When the amplitude is 0.25 mm, the application of vibration still decreases the time-averaged shear rate adjacent to the driving surface, but the decrement is less than that caused by the case when amplitude is 0.2 mm; moreover, although the time-averaged shear rate of the melt adjacent to the stationary surface increases in this case, the time-averaged shear rate of the melt that locates in the middle of the melt film decreases; thus, the promotion effect caused by this kind of VFF of too large vibration strength will not be proportional to the vibration strength applied.

From the above simulation results, it can be found out that even with the same VFF applied, the variation magnitude of the distribution of the time-averaged shear rate in the thinner melt film is larger than that in the thicker melt film. This phenomenon can be explained as follows. The average shear rate in the thin melt film is larger, the corresponding apparent viscosity becomes less, and the relaxation time also becomes shorter. For instance, when the thickness of thin melt film is one-fifth that of thick melt film, then the average shear rate in the thin melt film is five times that in the thick melt film; however, because the relationship between the shear rate and apparent viscosity is nonlinear, according to the Cross viscosity model eq. (15), the average apparent viscosity in the thin melt film is about one-third that in the thick melt film, namely, the average relaxation time of the melt in the thin melt film is about one-third that in the thick melt film. Thus, although the average relaxation time of the melt in the thin melt film is shorter, when the same VFF applied, because the average shear rate in the thin melt film is much more larger than that in the thick melt film, the nonlinear viscoelasticity response of the melt in the thin melt film is more intense than that in the thick melt film.

Results of temperature field

Figure 11(a) shows the curves of the difference between the time-averaged temperature distributions with various vibration parameters and temperature distribution without vibration in the thin melt film. When the amplitude is fixed (e.g., $a = 0.25$ mm) and the frequency is increased (e.g., from 5 to 15 Hz), the dissipation heat increases caused by the more and more strong effect of hysteresis, the time-averaged temperature increases, and the time-averaged temperature of the adiabatic surface is the highest. When the frequency is further increased to a certain large value (e.g., $f = 20$ Hz, $f = 25$ Hz), then the pulsant shear will decay to zero before reaching the adiabatic surface. A resting layer appears near the stationary surface where shear rate decreases and viscous dissipation heat reduces too, causing the time-averaged temperature near the adiabatic surface decrease, while the time-averaged temperature near the driving surface increase; since the driving surface is set to be at constant temperature, the heat of viscous dissipation generated near the driving surface will be conducted out from the driving surface and can not be used to melt the solid, which means that the energy is wasted; then there appears a strange phenomenon that with the further increase in the vibration strength; the time-averaged temperature near the solid/melt interface decreases instead. The above situation of time-averaged temperature increment is in accord with the variation situation of the time-averaged shear rate in the melt film, which indicates that the distribution of the time-averaged shear rate can be used to predict the distribution of time-averaged temperature. When the frequency is fixed, the effect of the increase in the amplitude on the time-averaged temperature distribution is similar to the effect of the increase in the frequency on the time-averaged temperature distribution while the amplitude is fixed.

Figure 11(b) shows the curves of the difference between the time-averaged temperature distributions with various vibration parameters and temperature distribution without vibration in the thick melt film. It can be seen that when the vibration strength is comparatively small ($f = 5$ Hz, $a = 0.25$ mm; $f = 25$ Hz,

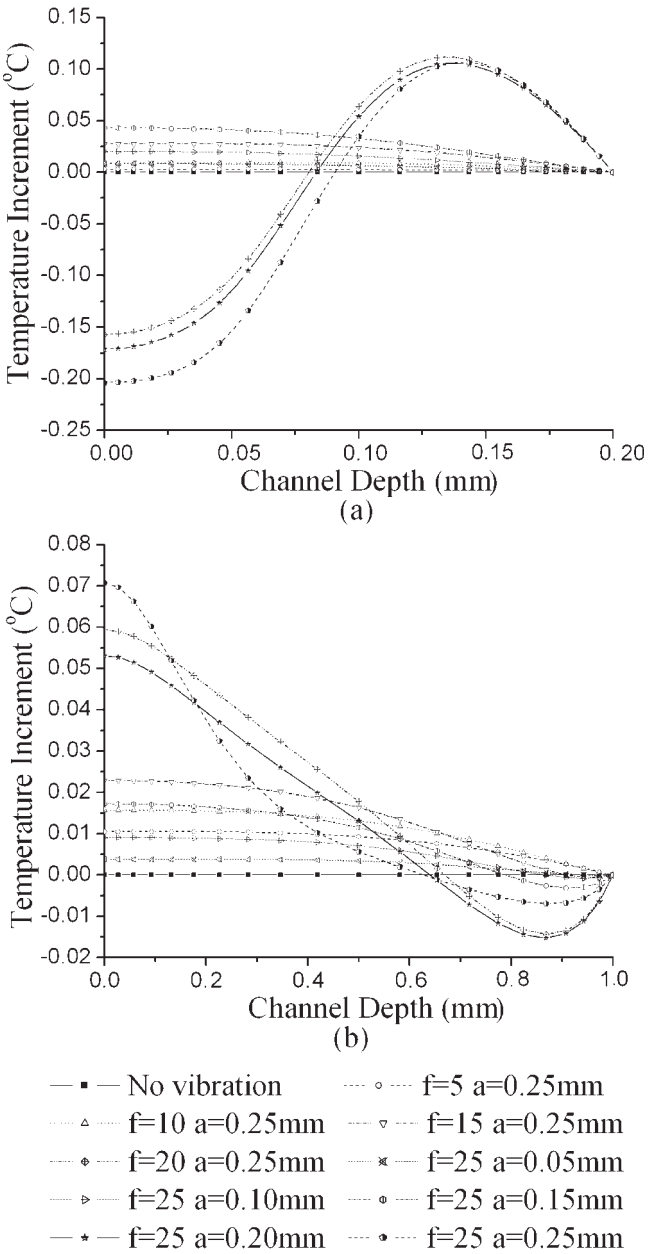

Figure 11 Curves of difference between time-averaged temperature distributions in the thin and thick melt films with various vibration parameters and temperature distribution without vibration, (a) $\delta = 0.2$ mm; (b) $\delta = 1$ mm.

$a = 0.05$ mm; $f = 10$ Hz, $a = 0.25$ mm; $f = 25$ Hz, $a = 0.10$ mm), the time-averaged temperature is higher than that without VFF caused by the dynamic dissipation heat due to the application of VFF. With the increase in the vibration strength ($f = 15$ Hz, $a = 0.25$ mm; $f = 25$ Hz, $a = 0.15$ mm; $f = 20$ Hz, $a = 0.25$ mm; $f = 25$ Hz; $a = 0.2$ mm), the time-averaged temperature of the melt adjacent to the driving surface drops a little, and the time-averaged temperature of the rest of the melt increases further. When the vibration strength is further increased ($f = 25$ Hz, $a = 0.25$ mm), the time-averaged temperature of the melt adjacent to the driving surface increases again, and the time-averaged temperature of the melt adjacent to the solid/melt interface also increases, but the increment of the time-averaged temperature of the melt in the middle of the melt film decreases. It is worth noting that it should take a period of time for the temperature distribution reaches steady status after the application of VFF, especially for a thicker melt film, it will take longer time for the temperature field to reach stable status; the durations from the moment of the application of VFF to the moment the temperature distribution reaching stable status are almost the same. Then, the period number needed to be calculated for a VFF with higher frequency (e.g., $f = 25$ Hz) will be much more than that needed to be calculated for a VFF with lower frequency, and the corresponding computing time will become much longer. In this work, the simulation results are all the results of the sixth period. For a VFF with lower frequency, the temperature field has almost reached the steady status, while for a VFF with higher frequency, especially for the cases that the frequency is 25 Hz, the temperature field has not reached the steady status yet.

Figure 12 shows the total average temperature variations in the thin melt film. Since it is easier for the temperature field of a thin melt film to reach the steady status, and thus, the simulation results of the thin melt film are all the results when the temperature fields have reached the steady status for the cases calculated, and those results are comparable. It can be seen that, the variation of the average temperature is not monotonous; there exists optimal combination of vibration parameters that can make the temperature of melt highest.

Figure 13 shows the total average temperature increments of the sixth period after the application of VFF in the thick melt film varying with amplitude, when the vibration frequency is 25 Hz. It can be seen that for the cases calculated in this work, the total average temperatures with various VFFs are all higher than that without VFF. When the amplitude increases from 0 to 0.15 mm, the total average temperature increment increases almost linear to the amplitude; when the amplitude increases from 0.15 to 0.2 mm, the temperature increases a little faster; but, when the amplitude further increases from 0.2 to 0.25 mm, the magnitude of temperature increment decreases instead. The relationship between the total average temperature increment and frequency is not presented here, because for the simulation results of the sixth period, the temperature results of higher frequency can not reach the steady state, and thus, those temperature increments can not be compared.

In addition, the comparison of the simulation results of the melt films of two different thicknesses shows that the effects of VFF to the melt of different melting stages are different. The optimum vibration strength of thin melt film is smaller than that of

thick melt film, because the melt in the thinner melt film behaviors stronger nonlinear viscoelastic characteristic than the melt in the thicker melt film does with the same VFF. Taking Figures 12(b) and 13 for example, when the amplitude is smaller than 0.15 mm, the total average temperatures of both the thin melt film and the thick melt film increase with the increase in amplitude; however, when the amplitude becomes larger than 0.15 mm, the average temperature of thin melt film decreases, while the average temperature of thick melt film still increases. Because the thickness of melt film keeps changing during the melting process; thus, for the smaller vibration strength, the average temperature of the melt film of various thickness during the melting process would increase with the increase in frequency and amplitude, which just corresponds to the experimental results of smaller vibration strength; for the larger vibration strength, the combined effects of temperature decrement in the thinner melt film and temperature increment in the thicker melt film result in the irregular variation of the melting rate, which corresponds to the experimental results of larger vibration strength. The theoretical results are qualitatively in agreement with the experimental results. Besides, the vibration parameters in the numerical simulation were larger than those in the experiments. The experiment results began to show irregular changes in melting length with smaller vibration parameters than the simulation results, which means that the actual average relaxation time reflected by the experiment is longer than the average relaxation time in the simulation; it is harder for the actual polymer melt to keep up with the variation of velocity caused by the application of the same VFF than for the simulation melt. We will try to eliminate the deviation of the relaxation time in the amended Maxwell model in our future work. However, the variation trend of the simulation results with the increase in frequency and amplitude coincide with that of the experiment qualitatively, which verified the validity of the simulation, and the simulation revealed the effect mechanism of the VFF on the melting process, although it is a simplified 2D melt film model. It is worth noting that because the melt film model does not take the solid phase into consideration, and the temperature boundary at the stationary surface is also different from the fact; the temperature results can only qualitatively reflect the comparative temperature variations caused by different vibration parameters.

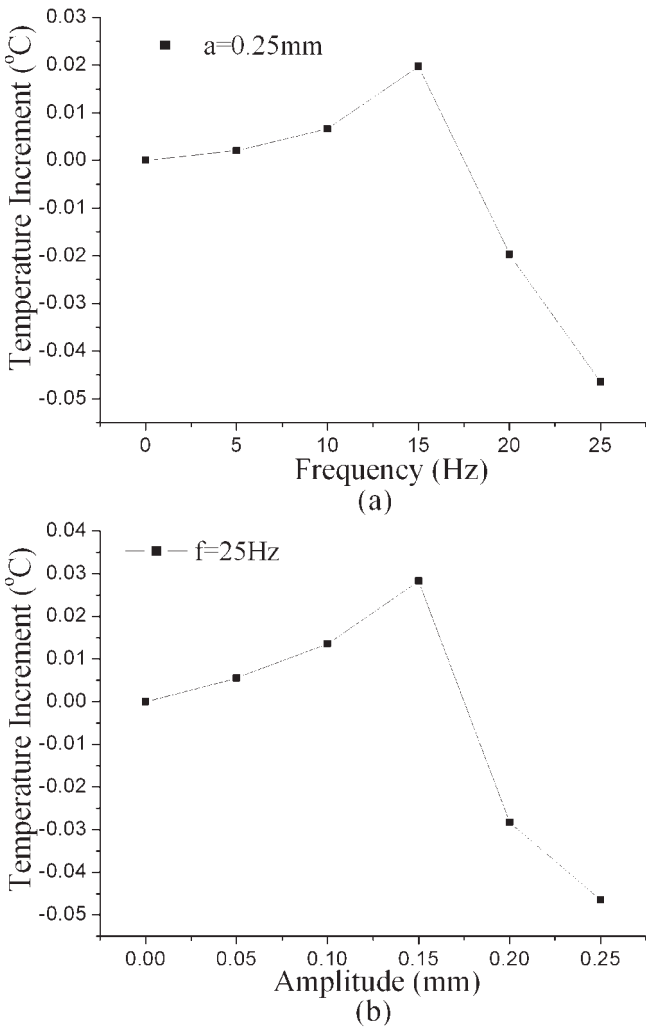

Figure 12 Total average temperature increment in the thin melt film, $\delta = 0.2$ mm, (a) $a = 0.25$ mm; (b) $f = 25$ Hz.

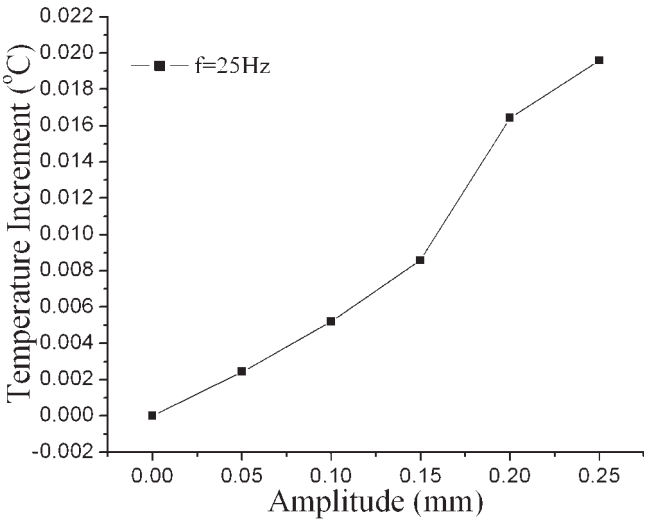

Figure 13 Total average temperature increment in the thick melt film varying with amplitude, $\delta = 1$ mm, $f = 25$ Hz.

CONCLUSIONS

To investigate the effect of VFF on the melting process in a VIPE, visualization experiments were carried out which revealed that there exit optimum vibration parameter combinations, when the vibra-

tion strength is smaller than the critical value determined by the rotate speed of screw, temperature settings of the barrel wall, the characteristic of die and the properties of material, the increase in vibration strength can further accelerate the melting rate; when the vibration strength exceed the critical vibration strength, the relationship between the melting rate and vibration strength becomes irregular.

A simplified 2D melt film model was established. The simulation results revealed that the effect of VFF on the temperature distribution during the melting process is implemented by the special variation of the melt conveying behavior caused by the VFF; thus, by investigating the dynamic conveying characteristic of the viscoelastic melt, the dynamic melting process can be investigated. Before the appearance of severe sudden change in velocity field, the application of VFF changes the shear rate distribution in the melt film, which transfer energy further to the solid/melt interface, instead of dissipating in the melt near the driving surface of which the temperature is relatively higher by outer heating, which can optimize the energy distribution, make the distribution of energy more even, and improve the utilization efficiency of energy. Thus, the larger the vibration amplitude and frequency are, the faster the melting rate becomes; when the vibration strength becomes higher than a certain critical value, which causes severe sudden change in velocity field, and causes the time-averaged shear rate of the melt near the driving surface increase and the time-averaged shear rate of the melt near the solid/melt interface decrease, then the energy can not be utilized to full advantage. This is a peculiar characteristic distinguishing the dynamic melting process from the conventional melting process. Therefore, there exist vibration parameter combinations to make the temperature distribution optimum. Because the melt in thinner melt film presents severer nonlinear viscoelastic behavior than the melt in thicker melt film with the same VFF, the critical vibration strength for thinner melt film is smaller than that for thicker melt film; and during the melting process, the melt film thickness keeps changing. Once the vibration strength exceed certain value, the combined effects of temperature decrement in the thinner melt film and temperature increment in the thicker melt film of the entire melting process result in the irregular variation of the melting rate. The theoretical prediction can explain the effects of VFF on the melting process observed in the visualization experiments qualitatively.

The melt film model put forward in this article can be conveniently used to study the dynamic response of the melt at any melting stage and any local position to the VFF. The study of the distributions of the dynamic velocity and temperature in the melt film can provide vigorous information for the prediction of the DMP. The analyses of dynamic responses of the melt of different melting stages and at different positions can also provide theoretical guidance for optimizing the vibration parameters for the DMP.

References

1. Casulli, J.; Clermont, J. R. Polym Eng Sci 1990, 30, 1551.
2. Wong, C. M.; Chen, C. H.; Isayev, A. I. Polym Eng Sci 1990, 30, 1574.
3. Isayev, A. I.; Wong, C. M.; Zeng, X. J Non-Newtonian Fluid Mech 1990, 34, 375.
4. Isayev, A. I.; Wong, C. M.; Zeng, X. Adv Polym Technol 1990, 10, 31.
5. Ibar, J. P. Polym Eng Sci 1998, 38, 1.
6. Chen, G.; Guo, S.; Li, Y. J Appl Polym Sci 2004, 92, 3153.
7. Chen, Y.; Li, H. J Appl Polym Sci 2005, 97, 1553.
8. Rahaman, K. D.; Ramkissoon, H. J Non-Newtonian Fluid Mech 1995, 57, 27.
9. Subbotin, A.; Semenov, A.; Hadziioannou, G.; Brinke, G. T. Macromolecules 1996, 29, 1296.
10. Orbey, N.; Dealy, J. M. J Rheol 1991, 35, 1035.
11. Wong, C. M.; Isayev, A. I. Rheol Acta 1989, 28, 176.
12. Adrian, D. W.; Giacomin, A. J. J Eng Mater Tech 1994, 116, 446.
13. Giacomin, A. J.; Oakley, J. G. J Rheol 1992, 36, 1529.
14. Jeyaseelan, R. S.; Giacomin, A. J. J Non-Newtonian Fluid Mech 1993, 47, 267.
15. Giacomin, A. J.; Jeyasseelan, R. S.; Samurkas T.; Dealy, J. M. J Rheol 1993, 37, 811.
16. Giacomin, A. J.; Jeyasseelan, R. S. J Eng Mater Tech 1994, 116, 15.
17. Giacomin, A. J.; Jeyasseelan, R. S.; Stanfill, K. O. Polym Eng Sci 1994, 34, 888.
18. Jeyaseelan, R. S.; Giacomin, A. J. J Non-Newtonian Fluid Mech 1994, 53, 99.
19. Giacomin, A. J.; Jeyasseelan, R. S. Polym Eng Sci 1995, 35, 768.
20. Atalık, K.; Keunings, R. J Non-Newtonian Fluid Mech 2004, 122, 107.
21. Qu, J. J South China Univ Tech (Natural science) 1992, 20, 1.
22. Qu, J. US Patent 5,217,302 (1993).
23. Wu, H.; Zhou, N.; He, H.; Qu, J. China Plast 1996, 10, 53.
24. Tadmor, Z. Polym Eng Sci 1966, 16, 185.
25. Shapiro, J.; Pearson, J. R. A.; Trottmow, R. Polymer 1978, 19, 1199.
26. Mount, E. M.; Watson, J. G.; Chung, C. I. Polym Eng Sci 1982, 22, 729.
27. Chung, K. H.; Chung, C. I. Polym Eng Sci 1983, 23, 191.
28. Rauwendaal, C. Adv Polym Technol 1992, 11, 19.
29. Cox, A. P. D.; Fenner, R. T. Polym Eng Sci 1980, 20, 562.
30. Chiew, L. M.; Gupta, M. J Reinforc Plast Compos 2002, 21, 1055.
31. Syrjälä, S. Int Comm Heat Mass Tran 2000, 27, 623.
32. Feng, Y.; Qu, J. Numerical Simulation of Melting Process in Vibration-induced Polymer Extruder, unpublished results.
33. Chang, R. Y.; Yang, W. L. J Non-Newtonian Fluid Mech 1994, 51, 1.
34. Ghoreishy, M. H. R.; Rafizadeh, M. Plast Rubber Compos Process Appl 1996, 25, 120.
35. Benoit, D. J Non-Newtonian Fluid Mech 2001, 98, 15.
36. Henrik, K. T. J Non-Newtonian Fluid Mech 1999, 84, 217.
37. Xue, S. C.; Tanner, R. I.; Phan-Thien, N. Comput Meth Appl Mech Eng 1999, 180, 305.
38. Baajijens, F. P. T. J Non-Newtonian Fluid Mech 1998, 79, 361.
39. Fan, Y.; Tenner, R. I.; Phan-Thien, N. J Non-Newtonian Fluid Mech 1999, 84, 233.
40. Adrian, D. W.; Giacomin, J. A. J Rheol 1992, 36, 1227.
41. Reimers, M. J.; Dealy, J. M. J Rheol 1996, 40, 167.
42. Debbaut, B.; Burhin, H. J Rheol 2002, 46, 1155.